Article

Neural Prediction of Tunnels' Support Pressure in Elasto-Plastic, Strain-Softening Rock Mass

Ali Ghorbani [1,*] (ID)**, Hadi Hasanzadehshooiili** [1] (ID) **and Łukasz Sadowski** [2] (ID)

[1] Department of Civil Engineering, Faculty of Engineering, University of Guilan, Rasht,
    Guilan 4199613776, Iran; h.hasanzadeh.shooiili@gmail.com
[2] Faculty of Civil Engineering, Wrocław University of Science and Technology, Wybrzeże Wyspianskiego 37,
    50-370 Wroclaw, Poland; lukasz.sadowski@pwr.edu.pl
[*] Correspondence: ghorbani@guilan.ac.ir; Tel.: +98-911-819-3170

check for updates

Featured Application: This work can be conjunctly used with the support characteristic curve of circular tunnels to find the optimum time of the installation of the support system in a way to restrict the displacements to a specific value. The approach described in this manuscript facilitates the design of circular tunnels for elasto-plastic, strain-softening rock masses obeying both Mohr–Coulomb and Hoek–Brown strength criteria.

Abstract: The prediction of the support pressure (P_i) and the development of the ground reaction curve (GRC) are crucial elements of the convergence–confinement procedure used to design underground structures. In this paper, two different types of artificial neural networks (ANNs) are used to predict the P_i of circular tunnels in elasto-plastic, strain-softening rock mass. The developed ANNs consider the stress state, the radial displacement of tunnel and the material softening behavior. Among these parameters, strain softening is the parameter of the deterioration of the material's strength in the plastic zone. The analysis also presents separate solutions for the Mohr–Coulomb and Hoek–Brown strength criteria. In this regard, multi-layer perceptron (MLP) and radial basis function (RBF) ANNs were successfully applied. MLP with the architectures of 15-5-10-1 for the Mohr–Coulomb criteria and 17-5-15-1 for the Hoek–Brown criteria appeared optimum for the prediction of the P_i. On the other hand, the RBF networks with the architectures of 15-5-1 for the Mohr–Coulomb criterion and 17-3-12-1 for the Hoek–Brown criterion were found to be the optimum for the prediction of the P_i.

Keywords: support pressure; radial displacement; ground reaction curve; circular tunnel; rock mass; elasto-plasticity; strain-softening; artificial neural network

1. Introduction

Convergence–confinement is a broadly applied method to design underground structures. In this method, a ground reaction curve (GRC) is applied to evaluate the interaction between the rock mass and the support system near the tunnel's face at the time of construction [1–3]. The classical problem of a circular tunnel constructed in the rock mass medium is illustrated in Figure 1b (according to [4]). This problem uses two well-known rock mass strength criteria: Mohr–Coulomb and Hoek–Brown. These criteria are usually adopted to investigate the behavior of materials. As described in references [4–6], the governing equilibrium equation of this problem is as presented in Figure 1d.
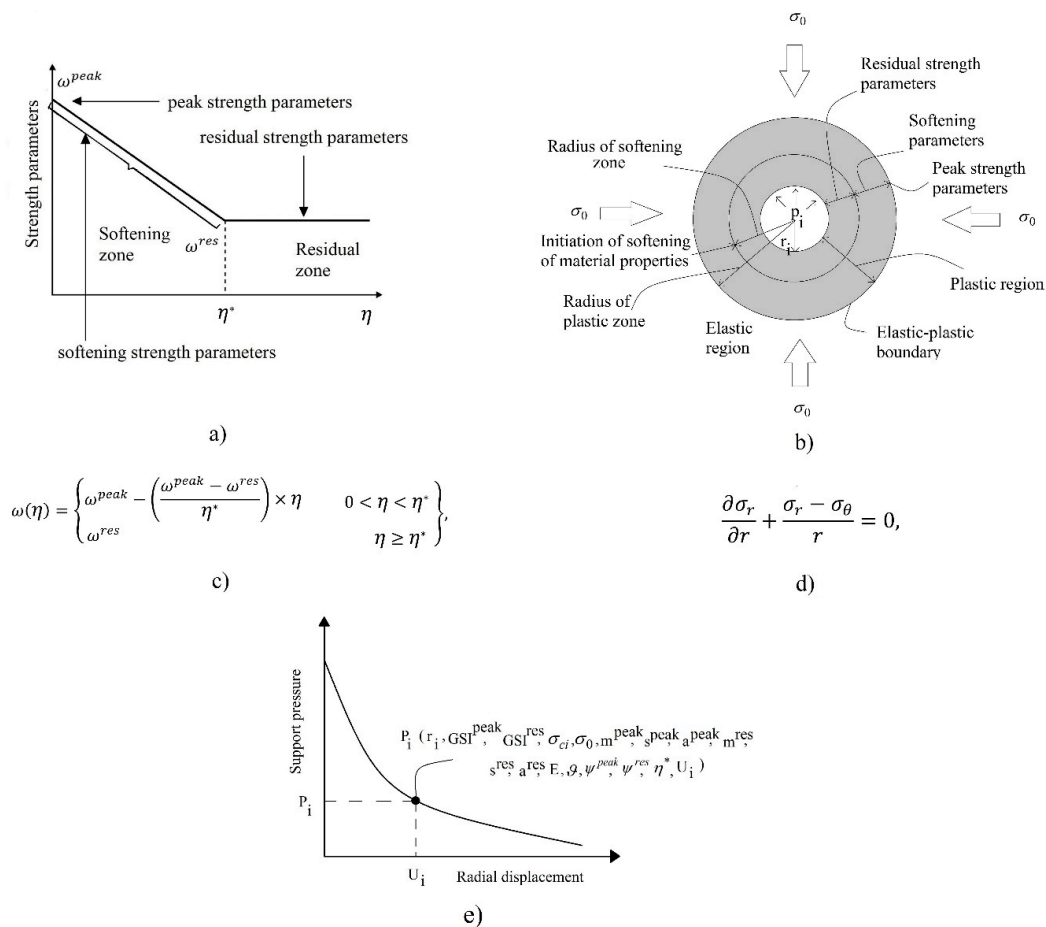
Figure 1. Description of: (**a**) different zones and corresponding strength parameters; (**b**) a circular tunnel in an elastic-plastic, strain-softening rock mass; (**c**) corresponding relationships for strength parameters; (**d**) governing equilibrium equation; (**e**) schematic view of a typical ground reaction curve (GRC) and parameters (Hoek–Brown case) affecting on the curve.

In Figure 1, σ_r is the radial stress, and σ_θ represents the tangential (hoop) stress, while the distance from the center of tunnel is shown using the r parameter. Thus, compatibility equations are simultaneously used to solve the stress–strain around the tunnel. In this regard, a plastic potential function and associated/non-associated flow rules are applied to find the governing relationship between the radial and tangential plastic strains [1,4,5,7–13]. The stress–strain around the tunnel is also calculated, considering the strength parameters in different zones (the peak, residual, and softening parameters), as presented in Figure 1a,c, according to reference [4]. As explained in reference [4], using different yield and potential functions, the non-associated flow rule is the modeled and adopted as the flow rule in all the cases. Also, starting from the peak strength parameters, the deterioration of the strength parameters of the material (referred to as the softening behavior of the rock mass around the tunnel) begins and continues. For softening parameter values higher than the critical value, the residual parameters are taken into the considerations. As shown in Figure 1a,c, $\omega(\eta)$ represents each of the strength parameters of the rock mass, and η and η^*, respectively, are the softening and the critical softening parameters. In this figure, σ_0 is the far-field in situ rock stress. In addition, Mohr–Coulomb and Hoek–Brown strength criteria are commonly used as two appropriate criteria to correctly evaluate the post-elastic behavior of rock mass. These criteria are, also, broadly applied in the literature for the development of the GRC. Hence, in this paper, available solutions with regard to the described problem are gathered, and rigorous datasets for both Mohr–Coulomb and Hoek–Brown strength criteria are obtained. As presented in the following sections, the collected

datasets are fed into the different types of artificial neural networks (ANNs). The main reason of ANN modeling of the tunnels' support pressure (P_i) is to save time and still obtain high accuracy in the predicted results. Previously, the evolutionary polynomial regression technique (EPR) was used by the authors to predict the P_i and to develop the GRC [4]. Nevertheless, there still exist some considerable prediction errors specially in the case of the Hoek–Brown strength criterion. Thus, we suppose that, in this case, ANNs may be more accurate. In this regard, available datasets should be sorted in the way shown in Figure 1e (a typical dataset for the case of the Hoek–Brown strength criterion). As depicted, each data pair stands for a point in the $U_i - P_i$ space. U_i is the tunnel's radial convergence and P_i represents the corresponding required internal P_i. Each of the described data is a function of some input parameters (the number of input parameters is determined on the basis of the type of the used strength criterion) and presents the P_i based on the all affecting parameters. For instance, in Figure 1e, P_i is a function of 17 independent input parameters.

The challenge is to predict the P_i of the internal support system [7–9,14]. The commonly known ways of P_i prediction employ different rock mass quality systems (e.g., rock mass rating, RMR; geological strength index, GSI, etc.) [15]. Some of these methods are also based on numerical codes, theoretical calculations, or coupled semi-analytical solutions [1,4,5,7,10–12,16–20]. Most of the commercial numerical packages, usually, use different finite element/difference codes [21]. These packages first define the element types, the material properties, and the geometry, together with the boundary and loading conditions. Discrete element packages are, also, used to model a rock medium containing specific joint sets with pre-defined orientations. All the described approaches are used to derive the governing differential equations and to present the solutions of the developed system [5,7,12]. Hence, they first need to be well validated against rigorous, available solutions and case studies. In addition, some of the existing methods have drawbacks (e.g., some of the available numerical solutions do not consider the deterioration of the strength parameters or do not correctly take the plastic straining into consideration [1]). Also, they require an adequate knowledge and background about the fundamentals and the theory of the convergence–confinement method and numerical and mathematical techniques. In addition to requiring an expert for the analysis, it is usually a time-consuming process to obtain the GRC. There are also other complex characteristics in the original problem which can be taken into the account, for instance, the material softening.

Considering the above, there is still a need to develop new methods for the reliable prediction of P_i in the elasto-plastic, strain-softening rock mass. In this regard, in this paper, the applicability of another new intelligent method of ANN modeling to predict the P_i of circular tunnels constructed in rock masses with different qualities is investigated.

The remainder of the paper is organized as follows. Section 2 presents the description of the research problems with background information, data acquisition, and the principles of different types of ANNs. Section 3 is the performance evaluation and compares the performance of ANNs with that of the previously proposed EPR models. Section 4, summarizes the results of the analyses.

2. Methodology

ANNs are broadly applied in engineering [22–29]. Also, over the last decades, ANNs have appeared as efficient meta-modelling methods applicable to a wide range of sciences, including material science and structural engineering [30–32]. An important characteristic of ANNs is that they can be used to build soft sensors, i.e., models with the ability to estimate critical quantities without having to measure them [30]. In particular, such alternative models are built after a training process with only a few available data, selected in a previous phase, to forecast the parameters. This considerably reduces the time and money needed for the experiments. One of the applicable fields of ANNs described in the literature is the prediction of the mechanical properties of concrete materials [33,34]. One of the main benefit of ANNs is that there is no need of any prior knowledge about the nature of the problem [35]. This makes ANNs applicable for a fast and reliable calculation of the P_i by practitioners who are not

expert in numerical modeling and programming. In this paper, two different types of ANNs, namely, the multi-layer perceptron (MLP) and the radial basis function (RBF), are applied to predict the P_i.

Data Acquisition

A dataset was compiled from input parameters for the Mohr–Coulomb and the Hoek–Brown criteria.

The datasets for the Mohr–Coulomb criteria were from reference [8]. A total of 168 independent input and output parameters and their range of variation are presented in Table 1. Although the datasets are those adopted from reference [8], the presented ANN models have the following superiority: When a new dataset is available, ANN helps to have a prediction based on the relationships they have found between previously used input and output parameters.

Table 1. Input and output parameters and their range of variation used in the prediction of the P_i (Mohr–Coulomb case).

Parameter	Range of Variation	Standard Deviation	Coefficient of Variation (%)
GSI^{peak}	21.4–64.9	17.48	34.45
GSI^{res}	15.1–33	6.91	26.20
σ_{ci}	23–162	60.09	60.49
γ	26–26.7	0.33	1.27
E	1.1–24	10.57	92.47
ϑ	0.25–0.3	0.02	8.27
c^{peak}	0.34–3.7	1.55	83.51
φ^{peak}	24.81–57.8	14.26	33.24
c^{res}	0.27–0.96	0.31	51.67
φ^{res}	15.69–51	15.42	42.51
m_i	10–20	4.47	27.61
ψ	0–14	6.14	90.30
σ_0	10.4–26	7.27	41.89
η^*	0.0465–0.1394	0.037	43.43
U_i	8.86–1263.69	307.86	147.24
P_i	0–2	0.55	71.55

GSI^{peak}: peak geological strength index, GSI^{res}: residual geological strength index, σ_{ci}: uni-axial compressive strength, γ: unit weight, E: Young's modulus, ϑ: Poisson's ratio, c^{peak} : peak cohesion, φ^{peak} : peak friction angle, c^{res} : residual cohesion, φ^{res} : residual friction angle, m_i: mi constant, ψ : dilation angle, σ_0 : in-situ rock stress, η^* : critical softening parameter, U_i : radial displacement, P_i : support pressure.

It should be noted that, in this table, the unit of U_i is mm, and the remaining parameters follow the units presented in the nomenclature.

Similar to the Mohr–Coulomb criteria, the dataset for the Hoek–Brown criteria was collected from the cases studied in references [5,6,9,36] and [14,37]. In total, 547 datasets were applied. Table 2 shows all the studied input and output parameters together with their range of variation. Differently from Table 1, in Table 2, the unit of U_i is m.

Table 2. Input and output parameters and their range of variation used in the prediction of the P_i (Hoek–Brown case).

Parameter	Range of Variation	Standard Deviation	Coefficient of Variation (%)
r_i	3–5.35	0.95	26.78
GSI^{peak}	25–100	29.52	41.34
GSI^{res}	10–100	35.89	67.07
σ_{ci}	27.6–75	22.83	42.59
E	1.38–36.51	9.03	112.80
ϑ	0.25	0	0
m^{peak}	0.5–4.09	0.94	57.06
s^{peak}	0.0002–0.0622	0.016	203.39
a^{peak}	0.5	0	0
m^{res}	0.1–1.173	0.29	41.75
s^{res}	0–0.002	0.00077	107.25
a^{res}	0.5–0.6	0.03	5.99
ψ^{peak}	0–30	9.38	84.71
ψ^{res}	0–20	5.50	94.45
σ_0	3.31–30	6.54	43.53
η^*	0.004742–100	34.66	216.12
U_i	0–0.282765	0.045	150.29
P_i	0–29.4	5.63	107.80

r_i : radius of tunnel, GSI^{peak}: peak geological strength index, GSI^{res}: residual geological strength index, σ_{ci}: uni-axial compressive strength, γ: unit weight, E: Young's modulus, ϑ: Poisson's ratio, m^{peak} : peak m constant, s^{peak} : peak s constant, a^{peak} : peak a constant, m^{res} : residual m constant, s^{res} : residual s constant, a^{res} : residual a constant, ψ^{peak} : peak dilation angle, ψ^{res} : residual dilation angle, σ_0 : in-situ rock stress, η^* : critical softening parameter, U_i : radial displacement, P_i : support pressure.

The multi-layer perceptron (MLP) ANN is still used by researchers in engineering [38]. The transfer function applied in this study is the TANSIG transfer function, according to the following formula:

$$TANSIG(e_x) = \frac{2}{1 + e^{(-2e_x)}} - 1, \tag{1}$$

where e_x is the weighted sum of the inputs for a neuron [39].

The radial basis function (RBF) ANNs are also popular in engineering. In RBF-ANN, by increasing the Euclidean distance between the input vector and its center, the output attained using the activation function will tend to zero. The width of RBF controls the decreasing rate of the output. Equation (2) shows the Gaussian basis function:

$$y_j = \exp\left(\frac{-\|\vec{x} - \vec{\mu}_j\|^2}{\sigma_j^2} \right), \tag{2}$$

3. Performance Evaluation

This section reports the evaluation of the performance of ANNs. It was conducted on the basis of the commonly known coefficient of determination (R^2), root-mean-square error ($RMSE$), and mean absolute error (MAE) [22,24,27,28,40–47].
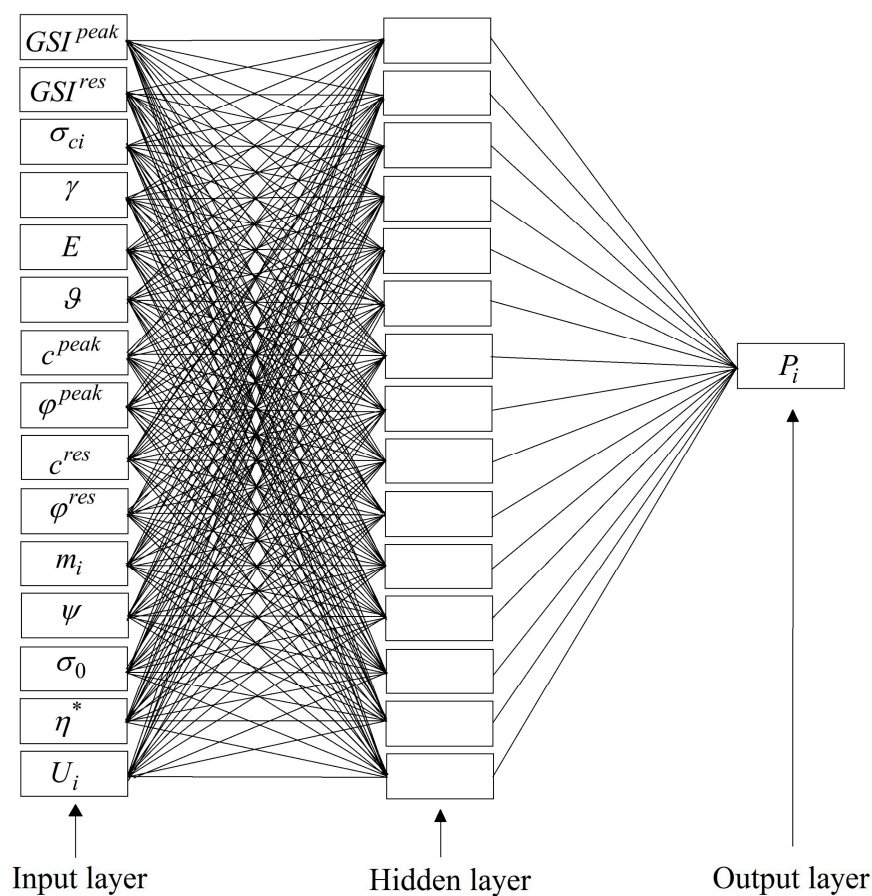
3.1. The Mohr–Coulomb Criterion

To evaluate the ANNs' performances, ANNs with different architectures and neurons were built. To do this, 70% of the total data fed into an ANN was used as the training dataset. The other remaining 30% was divided into two datasets, with 15% of the data used for cross-validation and 15% for testing. Then, the ANNs showing the best predictions (in terms of maximum R^2 and minimum $RMSE$ and MAE values) were selected. As shown in Table 3, the 15-5-10-1 and 15-15-1 networks were, respectively, the best MLP-ANN and RBF-ANN in the prediction of P_i for the Mohr–Coulomb strength criterion. In this case, the overall performance of MLP-ANN was better than that of the RBF-ANN.

Table 3. Performance of different multi-layer perceptron (MLP) and radial basis function (RBF) artificial neural networks (ANNs) in the prediction of the P_i for the testing data series (Mohr–Coulomb case).

Architecture	ANN Type					
	MLP-ANN			RBF-ANN		
	R^2 (%)	RMSE (MPa)	MAE (MPa)	R^2 (%)	RMSE (MPa)	MAE (MPa)
15-3-12-1	94.47	0.126617	0.09375	79.42	0.22383	0.1494
15-3-15-1	93.61	0.136705	0.100808	96.51	0.09361	0.06803
15-5-1	92.17	0.163929	0.102924	65.12	0.346439	0.256144
15-5-10-1	99.48	0.03883	0.02825	77.20	0.3193	0.2607
15-5-15-1	91.98	0.185252	0.128403	69.26	0.320201	0.180665
15-10-1	92.31	0.153122	0.110948	88.89	0.177232	0.142425
15-10-5-1	98.63	0.066325	0.042416	93.37	0.17276	0.124671
15-12-3-1	95.99	0.118647	0.06867	63.24	0.427169	0.340091
15-15-1	98.22	0.075068	0.058276	99.21	0.050576	0.040918
15-15-3-1	93.72	0.164167	0.107004	87.43	0.182931	0.140225
15-15-5-1	99.41	0.0459213	0.028215	81.90	0.255812	0.190918

RMSE: root mean squared error, MAE: mean absolute error.

Figure 2 (as a sample representative of the RBF-ANN) depicts the topology of the best RBF-ANN developed for the Mohr–Coulomb case (15-15-1 architecture with $R^2 = 99.21\%$, $RMSE = 0.050576$ MPa, and $MAE = 0.040918$ MPa). Figure 3a,b show the predicted P_i versus the calculated P_i.

Figure 2. The topology of the optimum RBF-ANN (15-15-1) developed for the prediction of the P_i (Mohr–Coulomb criterion).
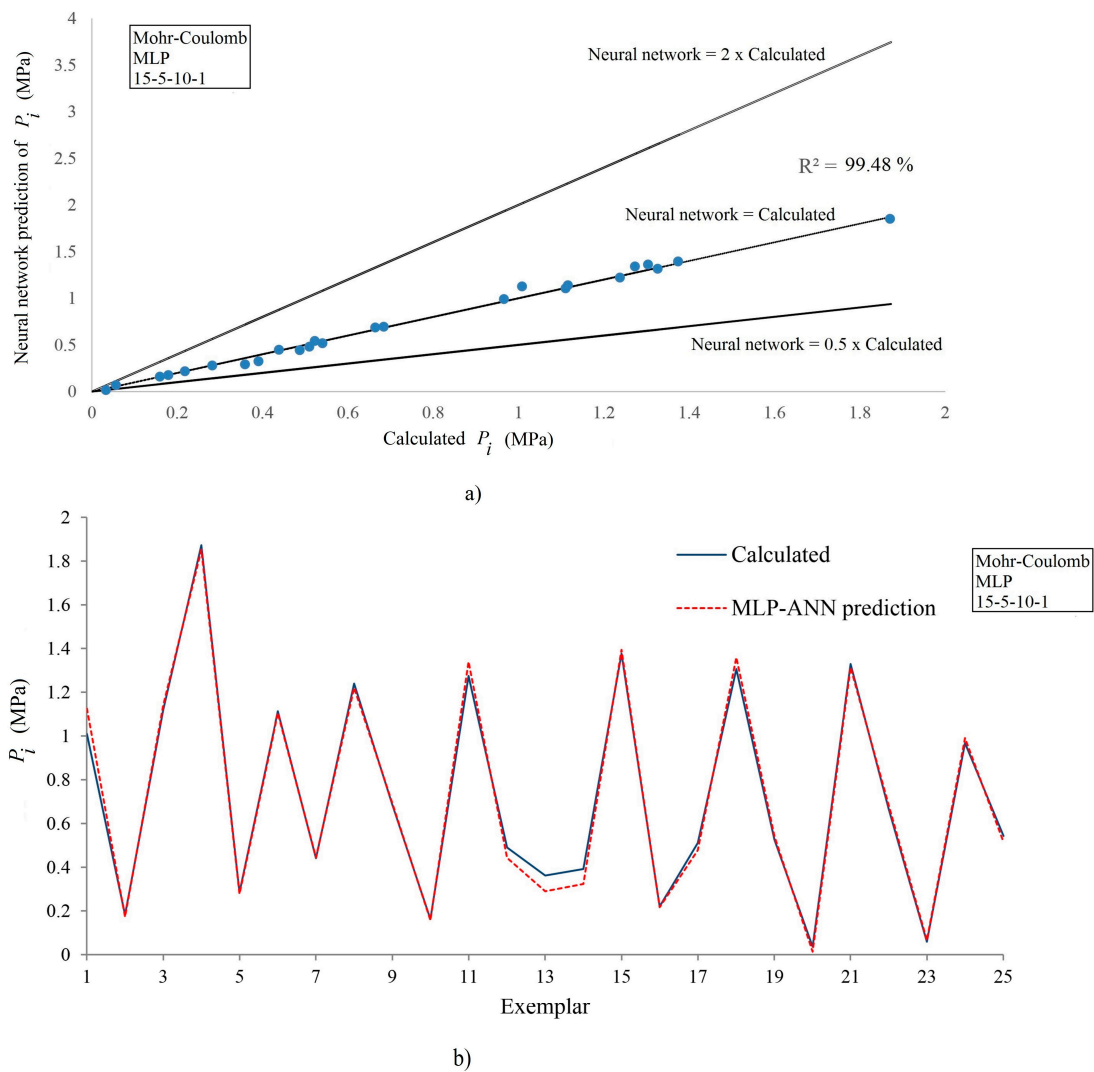
a)

b)

Figure 3. (**a**) ANN-based predicted P_i versus calculated P_i; (**b**) differences between ANN-based predicted P_i and calculated P_i for the best MLP-ANN (15-5-10-1) applied to the testing data series for the Mohr–Coulomb criterion.

Similar to Figure 3a,b, Figure 4a shows a high correlation between the calculated and the ANN-based prediction for the RBF-ANN in the case of Mohr–Coulomb strength criterion. Figure 4b, which better describes the occurred errors in the predictions for each sample, is another demonstration of the high capability of the proposed ANNs.
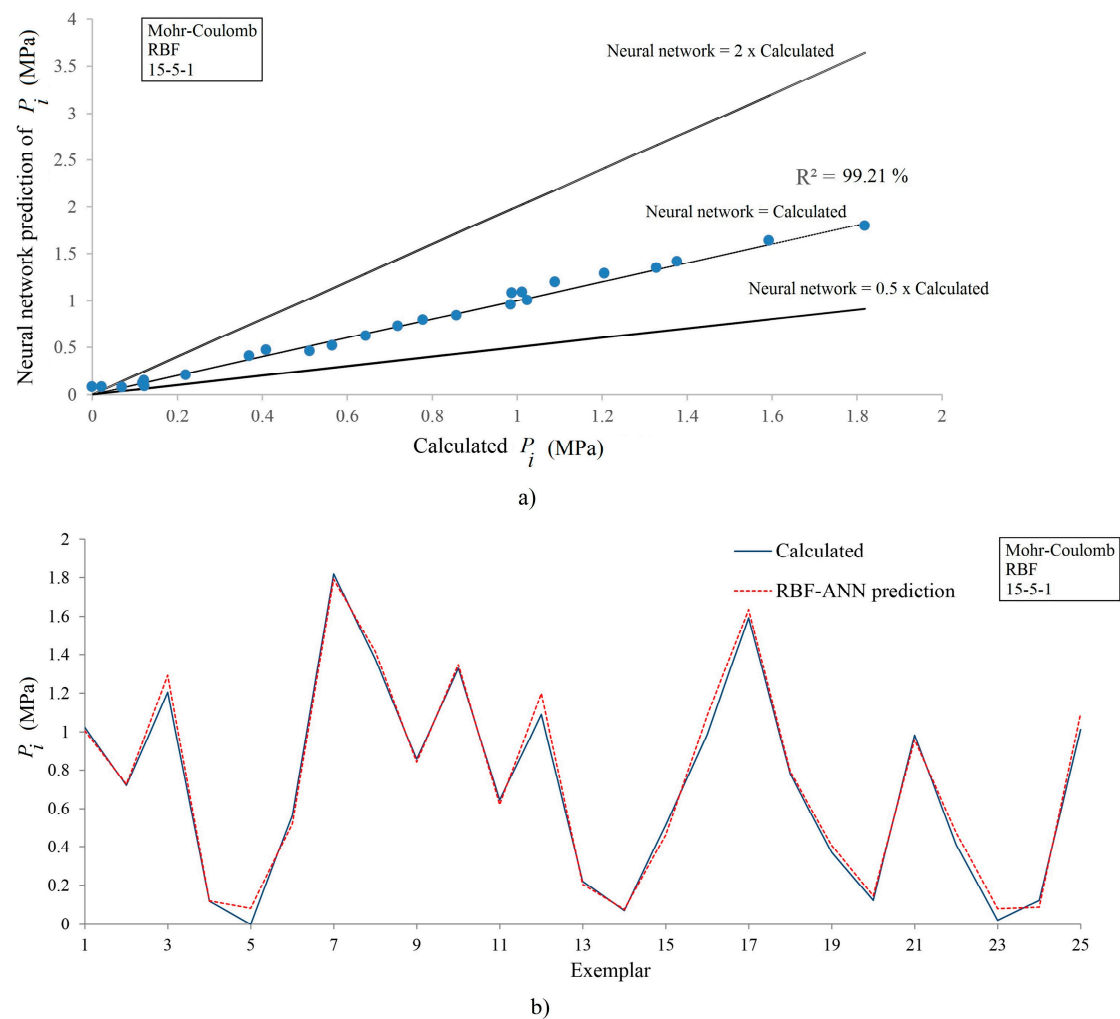
a)

b)

Figure 4. (**a**) ANN-based predicted P_i versus calculated P_i; (**b**) differences between ANN-based predicted P_i and calculated P_i for the best RBF-ANN (15-15-1) for the Mohr–Coulomb criterion.
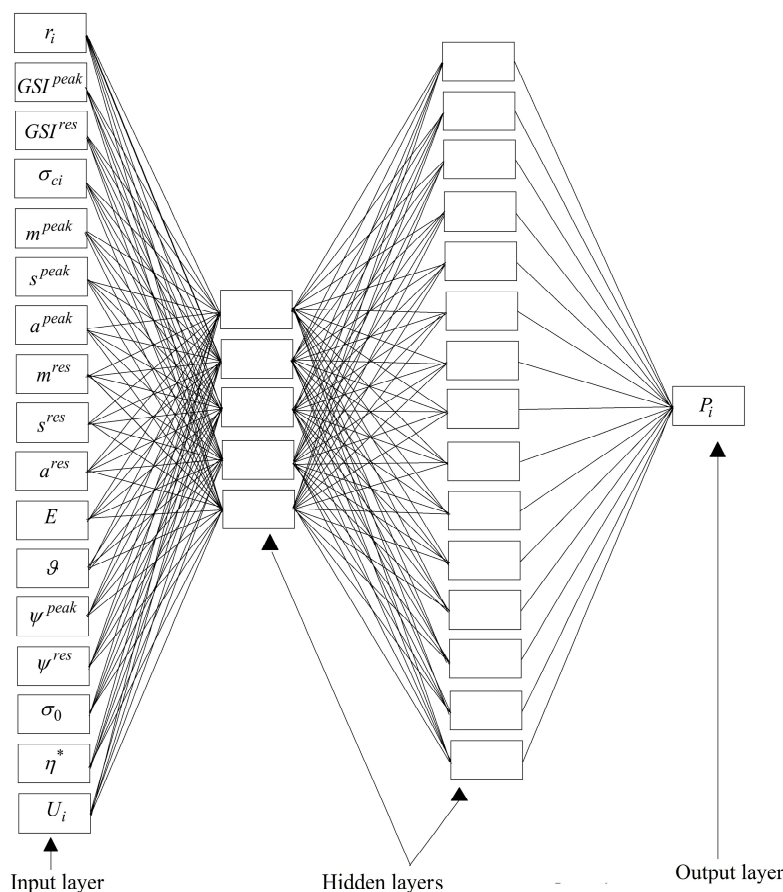
3.2. The Hoek–Brown Criterion

Similar to the Mohr–Coulomb case, the evaluation of the performance of ANNs was carried out on the 15% of the whole data series. By investigating different one- and two-layered neural ANNs, the 15-5-15-1 and 17-3-12-1 architectures were found to be the most efficient ANNs in the prediction of the P_i of tunnels in the Hoek–Brown case. As indicated in Table 4, the 17-5-15-1 MLP-ANN had a coefficient of determination of 99.91%, an *RMSE* of 0.179285 MPa, and a *MAE* of 0.12516 MPa. On the other hand, the most accurate RBF-ANN had an $R^2 = 93.18\%$, an $RMSE = 1.558064$ MPa, and a $MAE = 1.078099$ MPa. Although the developed ANNs for the Mohr–Coulomb case are more accurate compared to the Hoek–Brown case in terms of occurred errors, the ANNs suggested for the Hoek–Brown modeling were still useful and efficient. Also, it was shown that that MLP-ANN are more rigorous in the prediction of the P_i of circular tunnels excavated in the elasto-plastic, strain-softening, Hoek–Brown rock mass.

Table 4. Performance of different MLP and RBF ANNs in the prediction of the P_i for the testing data series (Hoek–Brown case).

| | ANN Type | | | | | |
| | MLP-ANN | | | RBF-ANN | | |
Architecture	R^2 (%)	RMSE (MPa)	MAE (MPa)	R^2 (%)	RMSE (MPa)	MAE (MPa)
17-3-12-1	99.72	0.268343	0.204655	93.18	1.558064	1.078099
17-3-15-1	93.37	1.36379	0.965679	84.51	2.515467	1.703367
17-5-1	99.63	0.317273	0.233694	78.35	2.570293	1.65224
17-5-10-1	90.37	1.565927	1.24049	89.05	2.165716	1.561432
17-5-15-1	99.91	0.179285	0.12516	87.72	1.810275	1.213031
17-10-1	99.67	0.300537	0.225826	77.64	2.497819	1.639146
17-10-5-1	99.87	0.252432	0.164251	80.62	2.627902	1.729953
17-12-3-1	99.80	0.239714	0.167833	88.72	2.06676	1.310764
17-15-1	99.65	0.322873	0.233356	90.51	1.877567	1.26464
17-15-3-1	99.85	0.20853	0.125573	77.22	3.019557	2.056784
17-15-5-1	99.72	0.307093	0.162638	72.15	3.060725	2.036629

The architecture and the topology of the most efficient MLP-ANN proposed for the modeling of the P_i in the Hoek–Brown case 17-5-15-1 is shown in Figure 5.

Figure 5. The topology of the optimum MLP-ANN (17-5-15-1) developed for the prediction of the P_i (Hoek–Brown criterion).

For the best constructed MLP-ANN, the predicted and calculated P_i, along with the relative differences of predictions and calculations for each independent exemplars are, respectively, shown in Figure 6. As clearly illustrated, the predictions are similar to the exact values of the calculations.

This result, which was generally observed also for the RBF networks (Figure 7), confirms that both MLP and RBF ANNs are highly applicable to the determination of the P_i.
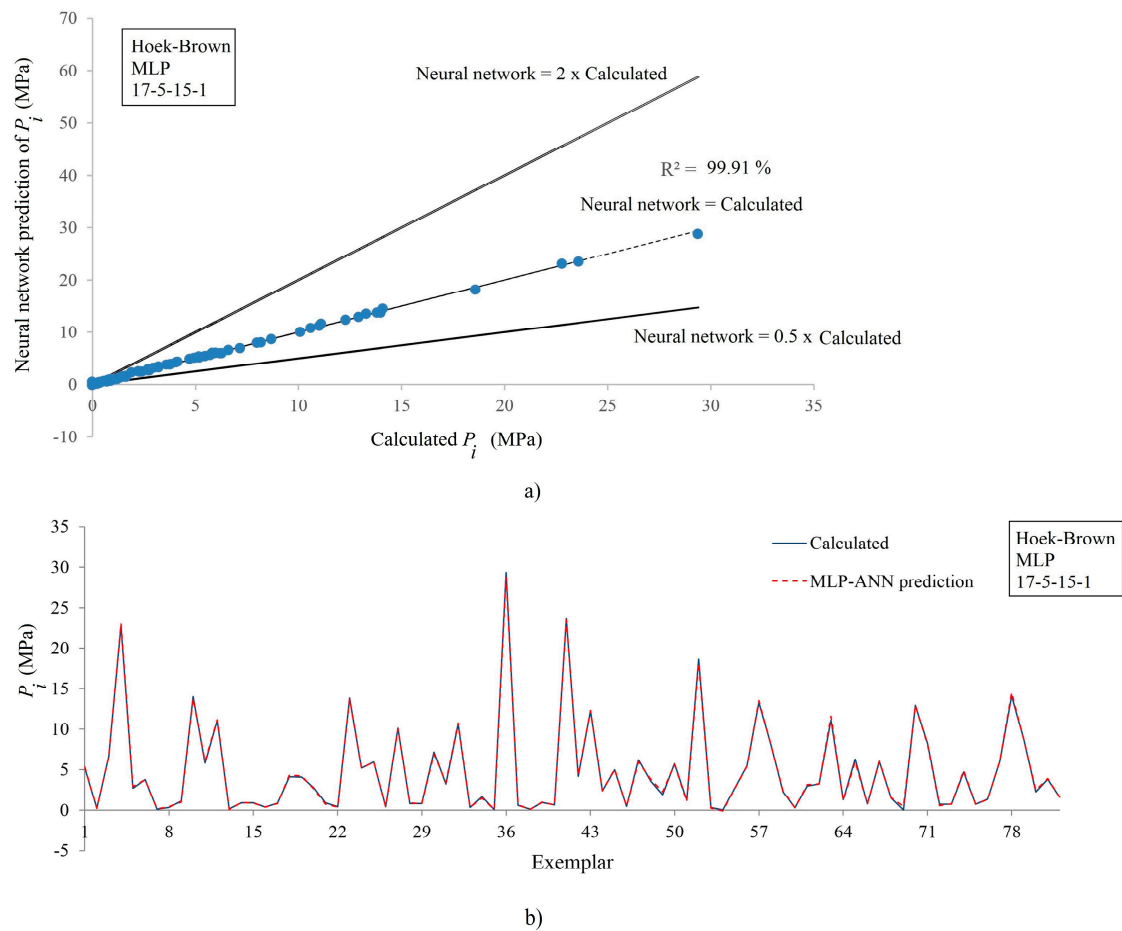

a)

b)

Figure 6. (**a**) Neural predicted P_i versus calculated P_i; (**b**) differences between neural predicted P_i and calculated P_i for the best MLP-ANN (17-5-15-1) applied to the testing data series for the Hoek–Brown criterion.
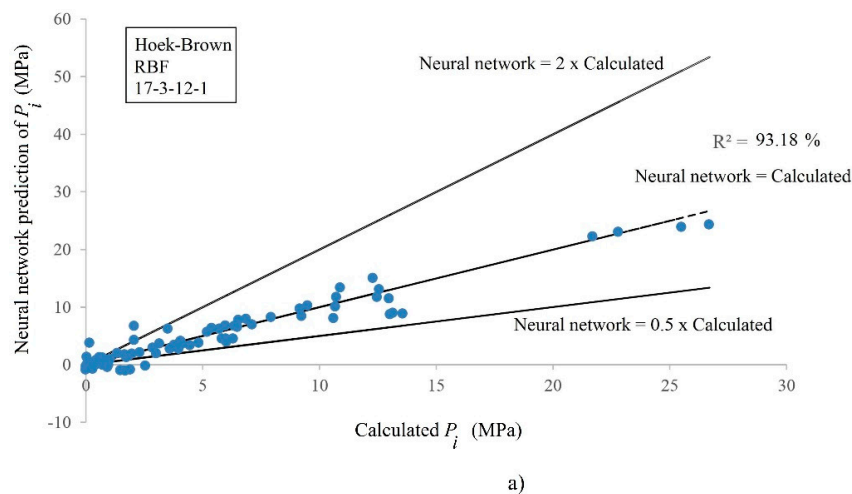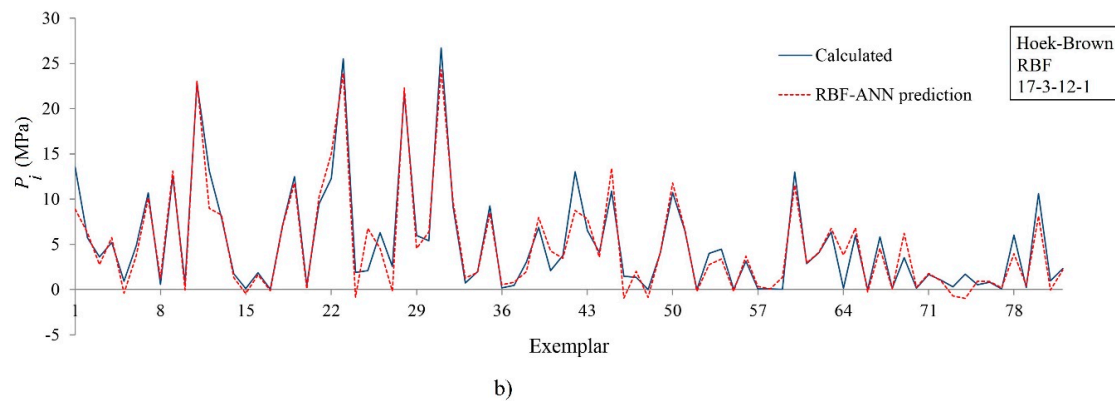

a)

Figure 7. *Cont.*

b)

Figure 7. (**a**) Neural predicted P_i versus calculated P_i; (**b**) differences between neural predicted P_i and calculated P_i for the best RBF-ANN (17-3-12-1) applied to the testing data series for the Hoek–Brown criterion.

3.3. Comparison with Previously Obtained Models

In this section, the performance of the developed ANNs is compared to that of a previous artificial intelligence (AI) technique developed by other authors [4], i.e., the evolutionary polynomial regression (EPR), for the prediction of P_i. In this regard, the testing data series used in each of the ANNs was fed into the predictive EPR models, and the P_i were approximated. The results of the comparison between the EPR and the ANN predictions are presented. On the basis of the results, all the proposed MLP and RBF ANNs predicted the pressures more accurately than the corresponding EPR models. As an example, Figure 8 compares the results obtained from an EPR model to those predicted by the 15-5-10-1 MLP-ANN for the case of Mohr–Coulomb criterion and by the 17-5-15-1 MLP-ANN for the case of Hoek–Brown strength criterion. As shown, all the performance's evaluation criteria presented higher accuracy in the ANN-based predictions than in the EPR model.
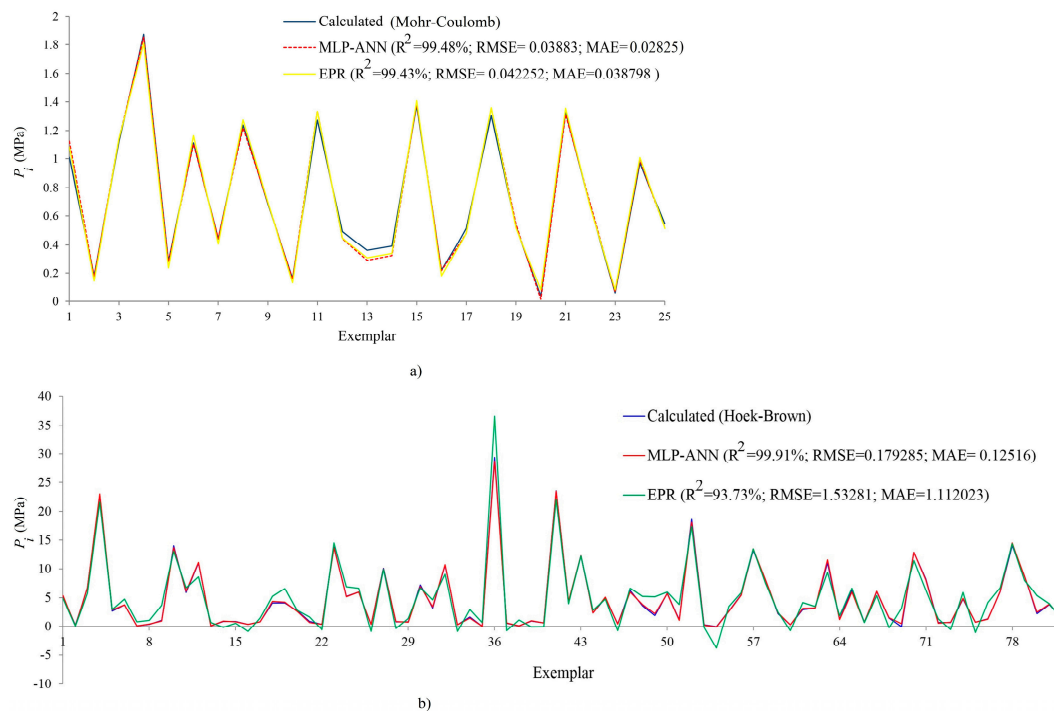
Figure 8. Comparison between the performance of (**a**) 15-5-10-1 MLP-ANN and evolutionary polynomial regression technique (EPR) model (Mohr–Coulomb case); (**b**) 17-5-15-1 MLP-ANN and EPR model (Hoek–Brown case) in the prediction of the P_i.

4. Conclusions and Perspectives

The available classical methods require a broad understanding of the governing mechanisms of the convergence–confinement method and programming skills to derive the GRC for the elasto-plastic, strain-softening rock mass. Considering the proven ability of AI techniques in the prediction of the P_i of circular tunnels [4], the applicability of another intelligent method is investigated in this study to obtain even more accurate predictions. To do this, the performance of two different ANN types, namely, MLP and RBF, were evaluated and compared. The described methods were applied to the GRC development in both the Mohr–Coulomb and the Hoek–Brown rock mass cases.

In this regard, available solutions with regard to the problem were collected, and a total of 168 and 547 datasets were compiled for the Mohr–Coulomb and the Hoek–Brown cases, respectively. Elastic rock mass properties, peak and residual strength parameters, softening and geometrical parameters, in situ stress, and the convergence of tunnel were employed as the input parameters to predict the internal P_i.

After building various one- and two-layer neural networks with the TANSIG transfer function and assessing the values of the coefficient of determination, root-mean-square error, and mean absolute error, the following conclusions were obtained:

- The ANN-based method appeared to be a highly performant method, applicable to the the development of GRC and the estimation of the P_i of circular tunnels;
- The 15-5-10-1 ($R^2 = 99.48\%$, $RMSE = 0.03883$ MPa, and $MAE = 0.02825$ MPa) and 15-15-1 ($R^2 = 99.21\%$, $RMSE = 0.050576$ MPa, and $MAE = 0.040918$ MPa) networks were reported as the best MLP and RBF networks for the Mohr–Coulomb case, respectively;
- For the Hoek–Brown case, the 17-5-15-1 MLP ($R^2 = 99.91\%$, $RMSE = 0.179285$ MPa, and $MAE = 0.12516$ MPa) and the 17-3-12-1 RBF ($R^2 = 93.18\%$, $RMSE = 1.558064$ MPa, and $MAE = 1.078099$ MPa) architectures were the most accurate proposed neural networks;

- It was shown that the overall performance of MLP networks was better than that of the RBF networks for both Mohr–Coulomb and Hoek–Brown cases;
- The results obtained from the comparison between neural network and EPR models proved the superiority of ANN to the EPR in the prediction of P_i;
- The proposed networks can be effectively applied by design engineers and practitioners to accurately, time-effectively, and economically obtain the GRC using a new set of data is available;
- The proposed networks can be successfully applied in conjunction with the support characteristic curve to calculate the proper time of the installation of the tunnels' supports;
- Regarding the successful application of ANNs to the problem and as suggestion for future works, the applicability of other soft computing techniques (e.g., genetic programming, ant or bee colony, etc.) can be investigated;
- As another perspective of the current research, stress–strain and time-dependent behavior of rock masses can be studied on the basis of the implementation of viscose constitutive models;
- The formation of damaged zones around the tunnel's surface (which is the subject of new work by the authors) and new EPR and ANN methods for the prediction of pressures are other interesting perspectives suggested by the present paper.

Author Contributions: The analyses were carried out by H.H. This paper was written by H.H., A.G. supervised the conducted research, reviewed, and revised the paper. Ł.S. reviewed, revised, and improved the paper.

Conflicts of Interest: The authors declare no conflict of interest.

Nomenclature

Symbol	Description	Unit	Symbol	Description	Unit
a^{res}	Residual a constant	[-]	w_j	Weight between neurons	[-]
a^{peak}	Peak a constant	[-]	$\vec{x}$	Input	[-]
c_i	Calculated value	[-]	y_j	Gaussian basis function	[-]
c^{peak}	Peak cohesion	MPa	γ	Unit weight	kN/m^3
c^{res}	Residual cohesion	MPa	η	Softening parameter	[-]
e_x	Weighted sum of the inputs	[-]	η^*	Critical softening parameter	[-]
E	Young's modulus	GPa	ϑ	Poisson's ratio	[-]
GSI^{peak}	Peak geological strength index	[-]	$\vec{\mu}_j$	Center of the Gaussian basis function	[-]
GSI^{res}	Residual geological strength index	[-]	σ_0	In-situ stress	MPa
MAE	Mean absolute error	[-]	σ_{ci}	Uni-axial compressive strength	MPa
m_i	mi constant	[-]	σ_j	Spread of the Gaussian basis function	[-]
m^{peak}	Peak m constant	[-]	σ_r	Radial stress	MPa
m^{res}	Residual m constant	[-]	σ_θ	Tangential stress	MPa
n	Number of datasets	[-]	φ^{peak}	Peak friction angle	°
p_i	Predicted value	[-]	φ^{res}	Residual friction angle	°
P_i	Support pressure	MPa	ψ	Dilation angle	°
r	Distance from the tunnel center	m	ψ^{peak}	Peak dilation angle	°
R^2	Coefficient of determination	[-]	ψ^{res}	Residual dilation angle	°
$RMSE$	Root-mean-square error	[-]	ω^{peak}	Peak strength parameters	[-]
s^{peak}	Peak s constant	[-]	ω^{res}	Residual strength parameters	[-]
s^{res}	Residual s constant	[-]	U_i	Radial displacement	m & mm
$TANSIG$	Tangent hyperbolic function	[-]			

References

1. Brown, E.; Bray, J.; Ladanyi, B.; Hoek, E. Ground response curves for rock tunnels. *J. Geotech. Eng.* **1983**, *109*, 15–39. [CrossRef]
2. Carranza-Torres, C.; Fairhurst, C. The elasto-plastic response of underground excavations in rock masses that satisfy the Hoek-Brown failure criterion. *Int. J. Rock Mech. Min. Sci.* **1999**, *36*, 777–809. [CrossRef]

3. Carranza-Torres, C.; Fairhurst, C. Application of the convergence-confinement method of tunnel design to rock masses that satisfy the Hoek-Brown failure criterion. *Tunn. Undergr. Space Technol.* **2000**, *15*, 187–213. [CrossRef]

4. Ghorbani, A.; Hasanzadehshooiili, H. A novel solution for ground reaction curve of tunnels in elastoplastic strain softening rock masses. *J. Civ. Eng. Manag.* **2017**, *23*, 773–786. [CrossRef]

5. Lee, Y.; Pietruszczak, S. A new numerical procedure for elasto-plastic analysis of a circular opening excavated in a strain-softening rock mass. *Tunn. Undergr. Space Technol.* **2008**, *23*, 588–599. [CrossRef]

6. Park, K.; Tontavanich, B.; Lee, J. A simple procedure for ground response of circular tunnel in elastic-strain softening rock masses. *Tunn. Undergr. Space Technol.* **2008**, *23*, 151–159. [CrossRef]

7. Alonso, E.; Alejano, L.R.; Varas, F.; Fdez-Manin, G.; Carranza-Torres, C. Ground response curves for rock masses exhibiting strain-softening behavior. *Int. J. Numer. Anal. Methods Geomech.* **2003**, *27*, 1153–1185. [CrossRef]

8. Alejano, L.R.; Rodriguez-Dono, A.; Alonso, E.; Fdez-Manin, G. Ground reaction curves for tunnels excavated in different quality rock masses showing several types of post-failure behavior. *Tunn. Undergr. Space Technol.* **2009**, *24*, 689–705. [CrossRef]

9. Alejano, L.R.; Alonso, E.; Rodriguez-Dono, A.; Fdez-Manin, G. Application of the convergence-confinement method to tunnels in rock masses exhibiting Hoek-Brown strain-softening behavior. *Int. J. Rock Mech. Min. Sci.* **2010**, *47*, 150–160. [CrossRef]

10. Zareifard, M.; Fahimifar, A. Analytical solutions for the stresses and deformations of deep tunnels in an elastic-brittle-plastic rock mass considering the damaged zone. *Tunn. Undergr. Space Technol.* **2016**, *58*, 186–196. [CrossRef]

11. Zou, J.-F.; Li, C.; Wang, F. A new procedure for ground response curve (GRC) in strain-softening surrounding rock. *Comput. Geotech.* **2017**, *89*, 81–91. [CrossRef]

12. Ghorbani, A.; Hasanzadehshooiili, H. A comprehensive solution for calculation of ground reaction curve of circular tunnels in elastic-plastic-EDZ rock mass considering strain softening. *Tunn. Undergr. Space Technol.* **2018**. under revision.

13. Ketabian, E.; Molladavoodi, H. Practical ground response curve considering post-peak rock mass behavior. *Eur. J. Environ. Civ. Eng.* **2017**, *21*, 1–23. [CrossRef]

14. Hoek, E.; Brown, E.T. Practical estimates of rock mass strength. *Int. J. Rock Mech. Min. Sci.* **1997**, *34*, 1165–1186. [CrossRef]

15. Santos, V.; da Silva, P.F.; Brito, M.G. Estimating RMR Values for Underground Excavations in a Rock Mass. *Minerals* **2018**, *8*, 78. [CrossRef]

16. Sharan, S. Analytical solutions for stress & displacements around a circular opening in a generalized Hoek-Brown rock. *Int. J. Rock Mech. Min. Sci.* **2008**, *45*, 78–85.

17. Wang, S.; Yin, X.; Tang, H.; Ge, X. A new approach for analyzing circular tunnel in strain-softening rock masses. *Int. J. Rock Mech. Min. Sci.* **2010**, *47*, 170–178. [CrossRef]

18. Gonzalez-Cao, J.; Varas, F.; Bastante, F.; Alejano, L. Ground reaction curves for circular excavations in non-homogeneous, axisymmetric strain-softening rock masses. *J. Rock Mech. Geotech. Eng.* **2013**, *5*, 431–442. [CrossRef]

19. Zareifard, M.; Fahimifar, A. Elastic-brittle-plastic analysis of circular deep underwater cavities in a Mohr-Coulomb rock mass considering seepage forces. *Int. J. Geomech.* **2015**, *15*. [CrossRef]

20. Park, K. Large strain similarity solution for a spherical or circular opening excavated in elastic-perfectly plastic media. *Int. J. Numer. Anal. Methods Geomech.* **2015**, *39*, 724–737. [CrossRef]

21. Pinheiro, M.; Emery, X.; Miranda, T.; Lamas, L.; Espada, M. Modelling Geotechnical Heterogeneities Using Geostatistical Simulation and Finite Differences Analysis. *Minerals* **2018**, *8*, 52. [CrossRef]

22. Baziar, M.H.; Ghorbani, A. Evaluation of lateral spreading using artificial neural networks. *Soil Dyn. Earthq. Eng.* **2005**, *25*, 1–9. [CrossRef]

23. Ghorbani, A.; Jafarian, Y.; Maghsoudi, M.S. Estimating shear wave velocity of soil deposits using polynomial neural networks: Application to liquefaction. *Comput. Geosci.* **2012**, *44*, 86–94. [CrossRef]

24. Hasanzadehshooiili, H.; Lakirouhani, A.; Medzvieckas, J. Superiority of artificial neural networks over statistical methods in prediction of the optimal length of rock bolts. *J. Civ. Eng. Manag.* **2012**, *18*, 655–661. [CrossRef]

25. Sadowski, Ł. Non-destructive evaluation of the pull-off adhesion of concrete floor layers using RBF neural network. *J. Civ. Eng. Manag.* **2013**, *19*, 550–560. [CrossRef]

26. Sadowski, Ł. Non-destructive investigation of corrosion current density in steel reinforced concrete by artificial neural networks. *Arch. Civ. Mech. Eng.* **2013**, *13*, 104–111. [CrossRef]

27. Hasanzadehshooiili, H.; Mahinroosta, R.; Lakirouhani, A.; Oshtaghi, V. Using artificial neural network (ANN) in prediction of collapse settlements of sandy gravels. *Arabian J. Geosci.* **2014**, *7*, 2303–2314. [CrossRef]

28. Sadowski, Ł.; Hoła, J. ANN modeling of pull-off adhesion of concrete layers. *Adv. Eng. Softw.* **2015**, *89*, 17–27. [CrossRef]

29. Ghorbani, A.; Hasanzadehshooiili, H. Prediction of UCS and CBR of microsilica-lime stabilized sulfate silty sand using ANN and EPR models; application to the deep soil mixing. *Soils Found.* **2018**, *58*, 34–49. [CrossRef]

30. Asteris, P.G.; Roussis, P.C.; Douvika, M.G. Feed-Forward Neural Network Prediction of the Mechanical Properties of Sandcrete Materials. *Sensors* **2017**, *17*, 1344. [CrossRef] [PubMed]

31. Asteris, P.G.; Plevris, V. Anisotropic masonry failure criterion using artificial neural networks. *Neural Comput. Appl.* **2017**, *28*, 2207–2229. [CrossRef]

32. Asteris, P.G.; Nozhati, S.; Nikoo, M.; Cavaleri, L.; Nikoo, M. Krill herd algorithm-based neural network in structural seismic reliability evaluation. *Mech. Adv. Mater. Struct.* **2018**, 1–8. [CrossRef]

33. Asteris, P.G.; Kolovos, K.G.; Douvika, M.G.; Roinos, K. Prediction of self-compacting concrete strength using artificial neural networks. *Eur. J. Environ. Civ. Eng.* **2016**, *20*, s102–s122. [CrossRef]

34. Asteris, P.G.; Kolovos, K.G. Self-compacting concrete strength prediction using surrogate models. *Neural Comput. Appl.* **2017**, 1–16. [CrossRef]

35. Funahashi, K.I. On the approximate realization of continuous mappings by neural networks. *Neural Netw.* **1989**, *2*, 183–192. [CrossRef]

36. Zareifard, M.; Fahimifar, A. A new solution for shallow and deep tunnels by considering the gravitional loads. *Acta Geotech. Slov.* **2012**, *2*, 37–49.

37. Cai, M.; Kaiser, P.K.; Tasakab, Y.; Minamic, M. Determination of residual strength parameters of jointed rock masses using the GSI system. *Int. J. Rock Mech. Min. Sci.* **2007**, *44*, 247–265. [CrossRef]

38. Yasrebi, S.S.H.; Emami, M. Application of Artificial Neural Networks (ANNs) in prediction and interpretation of pressuremeter test results. In Proceedings of the 12th International Conference of International Association for Computer Methods and Advances in Geomechanics (IACMAG), Goa, India, 1–6 October 2008.

39. Demuth, H.; Beal, M.; Hagan, M. *Neural Network Toolbox 5 User's Guide*; The Math Work, Inc.: Natick, MA, USA, 1996; 852p.

40. Girosi, F.; Poggio, T. Networks and the best approximation property. *Biol. Cybern.* **1990**, *6*, 169–176. [CrossRef]

41. Tawadrous, A.S.; Katsabanis, P.D. Prediction of surface crown pillar stability using artificial neural networks. *Int. J. Numer. Anal. Methods Geomech.* **2007**, *31*, 917–931. [CrossRef]

42. Heshmati, A.A.; Alavi, A.H.; Keramati, M.; Gandomi, A.H. A Radial Basis Function Neural Network Approach for Compressive Strength Prediction of Stabilized Soil. In Proceedings of the GeoHunan International Conference, Changsha, China, 3–6 August 2009.

43. Lashgari, A.; Fouladgar, M.M.; Yazdani-Chamzini, A.; Skibniewski, M.J. Using an integrated model for shaft sinking method selection. *J. Civ. Eng. Manag.* **2011**, *17*, 569–580. [CrossRef]

44. Sayadi, A.R.; Lashgari, A.; Paraszczak, J.J. Hard-rock LHD cost estimation using single and multiple regressions based on principal component analysis. *Tunn. Undergr. Space Technol.* **2012**, *27*, 133–141. [CrossRef]

45. Plevris, V.; Asteris, P.G. Modeling of masonry failure surface under biaxial compressive stress using Neural Networks. *Constr. Build. Mater.* **2014**, *55*, 447–461. [CrossRef]

46. Rafiei, M.H.; Khushefati, W.H.; Demirboga, R.; Adeli, H. Neural Network, Machine Learning, and Evolutionary Approaches for Concrete Material Characterization. *ACI Mater. J.* **2016**, *113*, 781–789. [CrossRef]

47. Golafshani, E.M.; Behnood, A. Application of soft computing methods for predicting the elastic modulus of recycled aggregate concrete. *J. Clean. Prod.* **2018**, *176*, 1163–1176. [CrossRef]